Letter

Data-driven configuration-interaction Hamiltonian extrapolation to ^{60}Ca

A. Magilligan [1,2] B. A. Brown [1,2] and S. R. Stroberg[3]

[1]*National Superconducting Cyclotron Laboratory, Michigan State University, East Lansing, Michigan 48824, USA*

[2]*Department of Physics and Astronomy, Michigan State University, East Lansing, Michigan 48824, USA*

[3]*Department of Physics, University of Washington, Seattle, Washington 98195, USA*

(Received 30 July 2021; accepted 19 October 2021; published 23 November 2021)

Following the many successful implementations of effective universal configuration-interaction Hamiltonians, we endeavored to produce a universal fp shell interaction tailored for the calcium isotopes, which we call UFP-CA. Starting from a state-of-the-art in-medium similarity renormalization group (IMSRG) interaction, linear combinations of Hamiltonian parameters that define the natural basis of the parameter space are constrained by the latest experimental data for the neutron-rich calcium isotopes. We show that this data-driven method for improving the Hamiltonian provides an excellent description of the known binding energies and spectra for the calcium isotopes within the fp model space. This together with comparisons to results from energy-density functional models leads us to conclude that ^{60}Ca is doubly magic at a similar level to ^{68}Ni. Several predictions are presented for unobserved low-lying excited states in $^{55-59}$Ca that will be accessible to future experiments.

DOI: 10.1103/PhysRevC.104.L051302

Next-generation experiments performed at newly built rare-isotope facilities will provide a greatly expanded view of the nuclear landscape. While qualitative predictions are available, quantitative predictions for those soon-to-be-discovered nuclei are needed to guide and motivate these experiments. In this Letter, we present a process to quantitatively describe the calcium isotopes out to ^{60}Ca, probably the last doubly magic nucleus to be discovered by the new radioactive-beam facilities.

Hamiltonians used for configuration-interaction calculations of nuclei are continually being improved. The *ab initio* based methods now include three-body interactions together with improved methods for handling short-ranged correlations and model space truncations [1] and are now able to describe binding energies within several MeV and energy spectra within about 500 keV. A recent example for the *sd* shell is shown in Ref. [1].

One can phenomenologically improve upon these interactions by using the energy data for nuclei in a given mass region to obtain effective two-body matrix elements (TBME) for a given model space. An effective method for doing this is to start with an *ab initio* based Hamiltonian and then to modify the best determined linear combinations (LC) of TBME that are required by the energy data using the singular value decomposition (SVD) method. The result is that both binding energies and energy spectra can be described to within 150–200 keV (see Fig. 9 of Ref. [1] and Fig. 5 of Ref. [2]).

The SVD method has resulted in widely used Hamiltonians for the *sd* model space [2,3], the fp model space [4–6], the mixed *sd* (protons) and fp (neutrons) model space [7], the *sd*-pf model space with particle-hole excitations [8,9], and the $jj44$ model space (see the Appendix in Ref. [10]). The relatively small modifications to the *ab initio* based TBME (on the order of up to 100–200 keV) reflect deficiencies in the many-body method, as well as the input $NN + 3N$ force.

We show that this data-driven method for improving the Hamiltonian provides an excellent description of the known binding energies and spectra for the calcium isotopes within the fp model space. The new universal fp interaction for calcium (UFP-CA) is presented in the Supplemental Material [11]. This together with comparisons to results from energy-density functional (EDF) models leads us to conclude that ^{60}Ca is doubly magic at a similar level to ^{68}Ni.

The data set used for this work contains the absolute binding energies for $^{46-57}$Ca, with the available experimental values from the 2016 Atomic Mass Evaluation [12] used for $A < 55$. Recently, the first mass measurements of $^{55-57}$Ca were published [13], and these are adopted here for the fit. Additionally, 23 well-known fp excited states are included in the fit as they contain important information for constraining the parameters involving the high-lying $0f_{5/2}$ and $1p_{1/2}$ orbits. Along with the 12 ground-state binding energies, our data set consists of 35 energy levels for these fp-shell calcium isotopes. Energies for $A < 46$ were excluded to avoid the influence of low-lying intruder states on the $0f_{7/2}$ parameters in the interaction. The excited states included in the fit are shown as green points at their experimental excitation energies in Fig. 1 along with a broad look at the energy spectra calculated with UFP-CA for the calcium isotopes with $A > 45$. Each line corresponds to a predicted energy level with the length and color representing the spin and parity of the level.

The fit begins by formulating the problem as a χ^2 minimization of N_p parameters p_j on a data set of size N_d:

$$\chi^2 = \sum_i^{N_d} w_i (E(\vec{p}) - E_i^{\mathrm{exp}}), \tag{1}$$

where the weights are set to $w_i = (\sigma_i)^{-2}$ with the adopted errors σ_i taken as the recorded experimental errors and a theoretical error added in quadrature. To normalize the minimized

 ©2021 American Physical Society

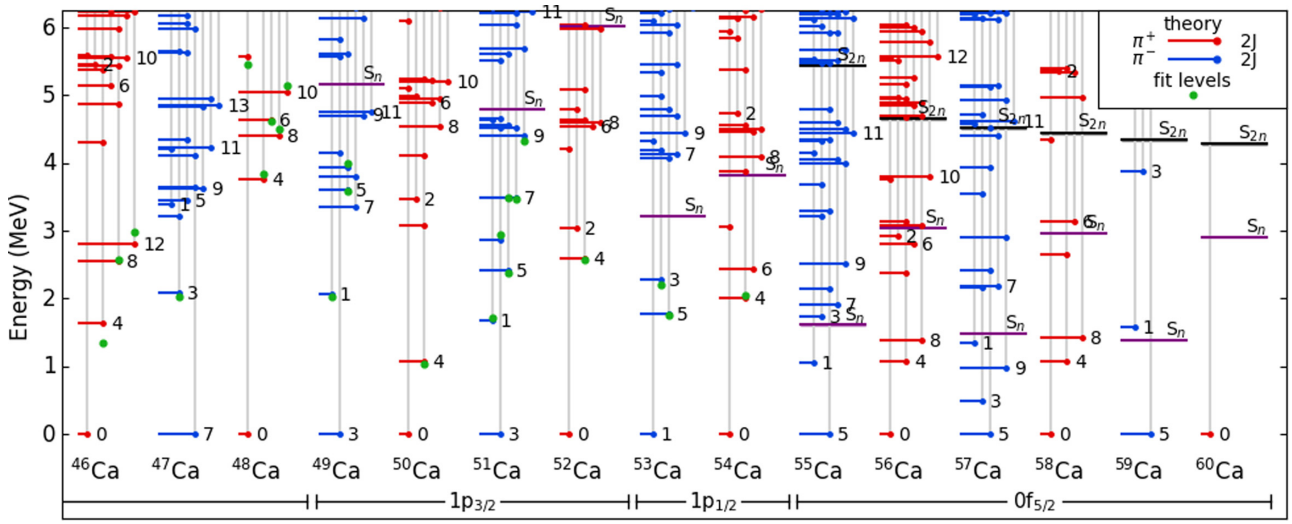

FIG. 1. Theoretical level schemes for neutron-rich calcium isotopes with $A > 45$ calculated using UFP-CA. Experimental excitation energies included in the fit are marked in green. Positive-parity states are shown in red, and negative-parity states are shown in blue. Each of these lines represents a level predicted to exist by the theory. Theoretical one- and two-neutron separation energies are shown as the purple and black lines, respectively.

χ^2 to the degrees of freedom $(N_d - N_p)$, we set $\sigma^{\text{th}} = 75$ keV. The χ^2 is minimized when $\vec{p} = \vec{p}_0$, which can be found using standard methods. However, the nuclear interaction parameters are highly correlated and the states included in this fit will be more dependent on some LC than others. This motivates us to truncate the parameter space.

Performing a SVD of the real symmetric data matrix (Eq. (9) in Ref. [3]) results in a diagonal matrix containing the singular values of the data matrix and a "rotation" matrix whose columns form an orthogonal basis that spans the parameter space. Small singular values correspond to poorly determined LC, which can be replaced with LC taken from an *ab initio* interaction p_s. This process is explained in depth in Ref. [3], and produces a family of solutions $\vec{p}_0(n)$, where n is the number of LC allowed to vary in the fit.

The parameter variance-covariance matrix S can be determined for each $\vec{p}_0(n)$ by inverting the singular value decomposition of the data matrix G, with the $i > n$ diagonal terms of the D matrix set to zero in order to capture only the statistical uncertainties from the regression. With $S(n)$, parameter uncertainties can be taken as $\Delta p_i(n) = \sqrt{S(n)_{ii}}$. This defines a "reasonable domain of model parameters" [14] around the minimum that provides interactions of similar quality to $\vec{p}_0$. Naturally then, the model-calculated observables, in this case binding and excitation energies, will have an acceptable range of values in this parameter domain. Using this, we can generate the statistical uncertainty introduced to the calculated energies at each n. At $n = 0$, these will be zero and tend to grow with n. The full uncertainty is a combination of the statistical uncertainty with the model uncertainty of around 100–200 keV for these effective interactions.

A reasonable starting interaction is needed for this procedure in order to effectively navigate the parameter space and maintain a physically grounded interaction. The calcium fp-shell data set allows us to think of our nuclei as a core of ^{40}Ca in its ground state with valence neutrons in the fp orbits. We construct a Hamiltonian for this system using a zero-body term (H_0), a one-body term (H_1), and a two-body term (H_2). H_0 is a fixed energy term set equal to the experimental energy of ^{40}Ca $(-342.052\,\text{MeV})$. H_1 is accounted for through single-particle energies, ϵ_α, for each neutron fp orbit α. For compatibility with the chosen H_0, we set these initially to the values found in the GPFX1A [4–6] interaction and then allow them to vary. As was done for the previous Hamiltonians in this region of the nuclear chart, ϵ_α are taken to be mass independent.

H_2 describes the interactions among the valence neutrons and contains the TBME, $v_{JT}(\alpha, \beta; \gamma, \delta)$, to be constrained. The TBME have a mass scaling of the form,

$$v_{JT}(ab; cd)(A) = \left(\frac{42}{A}\right)^p v_{JT}(ab; cd)(A = 42). \qquad (2)$$

The two-body nuclear strong interaction terms contained in H_2 scale with $p = 0.3$, consistent with Refs. [2,3,15]. Forces involving three or more nucleons are effectively constrained in $H_{1,2}$ by the fitting procedure. For this work, the TBME are set initially to values taken from a valence-space in-medium similarity renormalization group (VS-IMSRG) calculation [16]. Beginning with the EM1.8/2.0 $NN + 3N$ interaction [17] in an oscillator basis of frequency $\hbar\omega = 16$ MeV and $2n + \ell \leqslant e_{\max} = 14$, we normal order with respect to the Hartree-Fock ground state of ^{48}Ca and decouple the neutron fp valence space.

The limited size of our data set prevents us from fitting every TBME as the SVD of the full parameter data matrix fails. We limit our parameters to only the diagonal TBME and the ϵ_α for each fp orbit, the terms most impacted by three-body interactions and coupling to the continuum [18]. This gives us a total of 30 parameters p_i with which to perform the modified χ^2 minimization, as done in Ref. [2]. This family of solutions can be compared by examining their energy rms

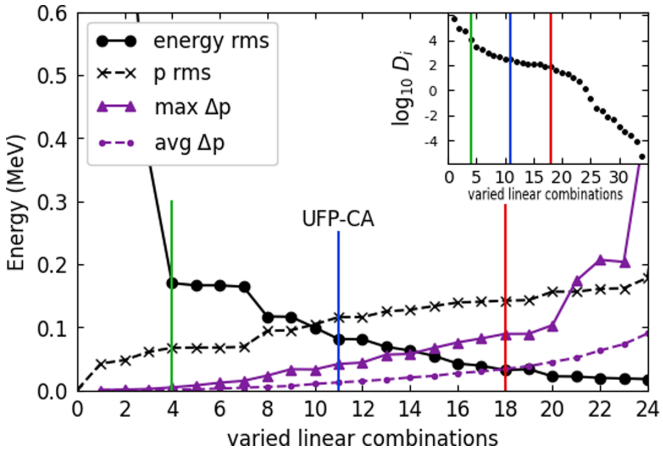

FIG. 2. Root-mean-square (rms) deviations plotted against varied LC. The black circles show the energy rms deviation between theory and experiment for the well-known levels included in the fit. The black crosses show the parameter rms deviation from the starting interaction. The average and maximum Δp are denoted by the purple triangles and points. The singular values are plotted on a log scale in the inset.

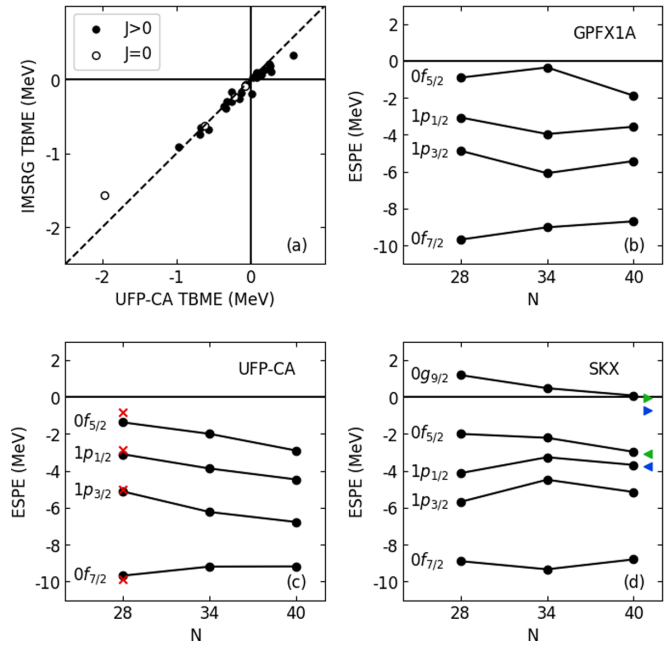

FIG. 3. A comparison of the TBME between UFP-CA and the initial IMSRG interaction is shown in panel (a). The ESPE discussed in the text are shown for GPFX1A (b), UFP-CA (c), and a Skyrme interaction (d). The red crosses show the IMSRG values at $N = 28$. The $0f_{5/2}$ (◁) and $0g_{9/2}$ (▷) are shown for the SKM* (green) and UNEDF0 (blue) EDF functionals.

deviations from the data set and the parameter rms deviations from the initial parameters. These results are shown in Fig. 2.

At $n = 4$ (green), there is a sharp drop in the energy rms deviation to around 180 keV, which indicates that the four ϵ_α are the most important parameters to achieve good agreement with experiment. The energy rms deviation continues to decline to around 30 keV; however, the maximum statistical uncertainty among the interaction parameters increases rapidly after $n = 20$, suggesting that the data are unable to constrain the interaction sufficiently after this point. To avoid this, we stop at $n = 18$ (red). The parameter rms deviation grows smoothly from around 60 keV at $n = 4$ to around 150 keV at $n = 18$. Results for the whole range of solutions from $n = 4$ to $n = 18$ are similar, and beyond $n = 11$ (blue) the improvements are very small.

As it is representative of our results, we choose the $n = 11$ solution as UFP-CA. The resulting single-particle energies and two-body matrix elements for $T = 1$ are given in the Supplemental Material [11]. The two-body matrix for $T = 0$ are taken from the GPFX1A Hamiltonian [4–6]. Figure 3 contains a scatter plot comparing the TBME in UFP-CA against the initial IMSRG interaction. The UFP-CA energy spectra for $^{46-60}$Ca are shown in Fig. 1 along with the one- and two-neutron separation energies. In addition to these states, unnatural-parity intruder states involving the $1s$-$0d$ orbits start at an excitation energy of 4 MeV near $A = 48$, and, in the weak-coupling model, intruder states involving and the $2s$-$1d$-$0g$ orbits will come as low as 1.4 MeV near $A = 60$.

There are several experimentally observed states with no definite spin assignment in this region that were not included in the fit. In ^{49}Ca, the National Nuclear Data Center (NNDC) reports the level at 3.354 MeV as $(9/2^+)$ but has recently been corrected to $7/2^-$ [19]. We predict a $7/2^-$ state at approximately this energy along with a second nearby $7/2^-$ state. Apart from this, there are nine levels with unknown spin in $^{49\text{-}55}$Ca that fall within 150 keV of our predictions. There are no known levels up to 5 MeV that are contrary to our predictions, except for the unnatural parity states and three states in ^{51}Ca only observed in one three-nucleon transfer reaction [20].

The calculated S_{2n} for UFP-CA are compared to experiment in the top panel of Fig. 4. We see excellent agreement with experiment for the separation energies across the shell, with expected minor deviations for ^{46}Ca and ^{40}Ca from mixing with low-lying intruder states. The bottom panel of Fig. 4 highlights the deviations from the UFP-CA predictions for experiment and several interactions: the GPFX1A interaction [4–6], results from Ref. [21] both with and without three-body correlations, and results from using nuclei-specific IMSRG interactions [16]. These theories all predict significantly lower S_{2n} at the top of the $f_{5/2}$ shell. Other previous theoretical work on the neutron-rich calcium isotopes using *ab initio* methods include Refs. [22–26].

Our results indicate that the calcium isotopes are stable to neutron decay out to ^{60}Ca as observed experimentally [27]. There are three sources of uncertainty in the extrapolation out to ^{60}Ca. First, the quality of the reproduction of the experimental data for $n = 11$ varied linear combinations within fp model space leads to statistical uncertainties on the energies on the order of 90 keV. Second, the predictions beyond ^{56}Ca rely on the IMSRG model for the $0f_{5/2}$ TBME that are not constrained by data. The rms deviation between the UFP-CA and IMSRG TBME, see Fig. 2, is 120 keV. This implies that the uncertainty in the energies within the fp model space from

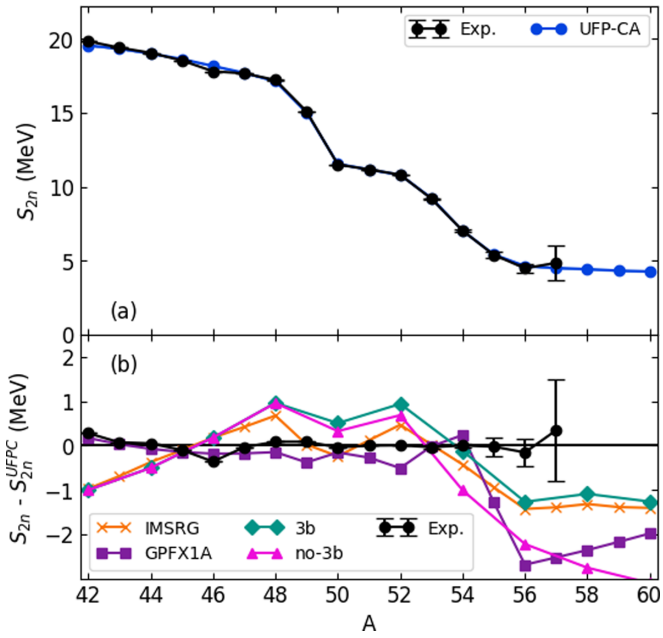

FIG. 4. Experimental and calculated S_{2n} for the calcium isotopes. See text for a description of the bottom panel.

^{56}Ca to ^{60}Ca is about 120 keV. The third source of uncertainty is the adequacy of the fp model space. For this, we rely on the observation that all of the known energy data can be described by an effective set of TBME within the fp model space and that these TBME are close to those predicted by the IMSRG calculations. The most critical test will be new experimental data from ^{56}Ca to ^{60}Ca. An interesting detail is the presence of 4^+ states in ^{56,58}Ca with dominant $(0f_{5/2})^{2,4}$ configurations with a predicted lifetime of about 20 ns.

The renormalization of the fp Hamiltonian implicitly contains the effects from sdg admixtures. This means that the shell gap between fp and sdg orbitals at $Z = 28$ and $N = 40$ is large enough to prevent the 2p-2h configurations from becoming ground states as they do in the islands of inversion [28]. The known regions of islands of inversion involve deformations driven by the proton-neutron interaction. Thus, ^{54}Cr and ^{56}Fe are known to be inside the $N = 40$ island of inversion. Is there an island of inversion for ^{60}Ca? A signature would be if $^{58-60}$Ca are more bound than we predict. Low-lying excited states not described by our predictions will also give direct information on the location of the $0g_{9/2}$, $1d_{5/2}$, and $2s_{1/2}$ orbitals.

An important goal of this work is to determine whether ^{60}Ca can indeed be treated as a closed shell. This designation is dependent on the magnitude of the energy gap between the $0f_{5/2}$ orbit and the $0g_{9/2}$ orbit. As our model space does not include this orbit, we extrapolate through comparisons to energy-density functional (EDF) calculations. To allow intermodel comparisons, we introduce the "effective" single particle energies (ESPE) that evolve with the nuclear mass. These are a combination of the TBME and ϵ_α for the one-particle and one-hole configurations around a closed shell at $N = 28$, 34, and 40. The four ESPE calculated with GPFX1A and UFP-CA are plotted in Figs. 3(b) and 3(c).

The shell gap can be inferred from EDF calculations based on a closed-shell configuration for ^{60}Ca. The EDF can be tested against the ESPE we obtain from the binding energy differences of ^{60}Ca and ^{59}Ca with one hole in fp.

The ESPE for ^{48,56,60}Ca obtained with the Skx functional [29] are shown in Fig. 3(d). In the Mass Explorer [30], binding energies of ^{61,60,59}Ca are given for the SKM* [31] and UNEDF0 [32] models. The results implied for the $0f_{5/2}$ and $0g_{9/2}$ ESPE are shown on the right-hand side of Fig. 3(d). The EDF ESPE agree with UFP-CA ESPE within about 1 MeV. This is similar to the differences between Skx EDF and experimental ESPE observed for other doubly magic nulcei [29]. All of these comparisons point to a gap of about 3 MeV between the $0f_{5/2}$ and $0g_{9/2}$ in ^{60}Ca within an uncertainty of about 1 MeV. The ESPE gap for ^{68}Ni obtained with the Hamiltonian in Ref. [33] is 1.95 MeV. Therefore, we expect the properties around ^{60}Ca to be comparable to those around ^{68}Ni.

For ^{61}Ca, $S_{1n} = e_9$ where e_9 is the single-particle energy of the $0g_{9/2}$ orbital. With Skx, e_9 is near zero energy, and ^{61}Ca may or may not be bound. For ^{62}Ca $S_{2n} = 2e_9 + V_0$, where V_0 is the effective TBME for $0g_{9/2}^2, J = 0$ which is on the order of 2 MeV. Thus ^{62}Ca is likely to be inside the neutron drip line. These conclusions are in line with the Bayesian model averaging results of Neufcourt *et al.* [34], which predict a bound ^{60}Ca with $S_{2n} = 5(1)$ MeV and report an existence probability of 46% for ^{61}Ca. They further conclude that even-even calcium isotopes out to $A = 70$ are likely to exist.

Lenzi *et al.* [35] have extrapolated the neutron effective single-particle energies from $Z = 28$ down to $Z = 20$ based on their LNPS Hamiltonian. Their $0f_{5/2}$-$0g_{9/2}$ ESPE gap for ^{60}Ca is close to zero (see Fig. 1 in Ref. [35]), in contrast to the EDF gaps of about 3 MeV. As shown in Ref. [36], the ESPE of the $0g_{9/2}$ has a strong influence on the structure of $^{56-60}$Ca that can be tested by experiment.

We have presented UFP-CA, a new interaction tailored to the fp shell calcium isotopes, based on the best available experimental data. Using this, we have presented extrapolated predictions out the ^{60}Ca and compared those results to experiment and other theoretical works. Our extrapolation along with comparisons to EDF calculations implies that ^{60}Ca is likely doubly magic at a level similar to ^{68}Ni. However, this is ultimately a question that will be decided by experiment. To further refine a shell model view of this isotopic chain, more experimental data involving the $0f_{5/2}$ and the $0g_{9/2}$ orbits is needed.

We acknowledge support from National Science Foundation Grants No. PHY-1811855 and No. PHY-2110365. S.R.S. is supported by the U.S. Department of Energy under Contract No. DE-FG02-97ER41014.

[1] S. R. Stroberg, H. Hergert, S. K. Bogner, and J. D. Holt, Annu. Rev. Nucl. Part. Sci. **69**, 307 (2019).

[2] A. Magilligan and B. A. Brown, Phys. Rev. C **101**, 064312 (2020).

[3] B. A. Brown and W. A. Richter, Phys. Rev. C **74**, 034315 (2006).
[4] M. Honma, T. Otsuka, B. A. Brown, and T. Mizusaki, Phys. Rev. C **65**, 061301(R) (2002).
[5] M. Honma, T. Otsuka, B. A. Brown, and T. Mizusaki, Phys. Rev. C **69**, 034335 (2004).
[6] M. Honma, T. Otsuka, B. A. Brown, and T. Mizusaki, Eur. Phys. J. A **25**, 499 (2005).
[7] Y. Utsuno, T. Otsuka, B. A. Brown, M. Honma, T. Mizusaki, and N. Shimizu, Phys. Rev. C **86**, 051301(R) (2012).
[8] R. S. Lubna, K. Kravvaris, S. L. Tabor, V. Tripathi, A. Volya, E. Rubino, J. M. Allmond, B. Abromeit, L. T. Baby, and T. C. Hensley, Phys. Rev. C **100**, 034308 (2019).
[9] R. S. Lubna, K. Kravvaris, S. L. Tabor, V. Tripathi, E. Rubino, and A. Volya, Phys. Rev. Research **2**, 043342 (2020).
[10] S. Mukhopadhyay, B. P. Crider, B. A. Brown, S. F. Ashley, A. Chakraborty, A. Kumar, M. T. McEllistrem, E. E. Peters, F. M. Prados-Estévez, and S. W. Yates, Phys. Rev. C **95**, 014327 (2017).
[11] See Supplemental Material at http://link.aps.org/supplemental/10.1103/PhysRevC.104.L051302 for a table of the UFP-CA single-particle energies and the two-body matrix elements.
[12] G. Audi, F. G. Kondev, M. Wang, W. Huang, and S. Naimi, Chin. Phys. C **41**, 030001 (2017).
[13] S. Michimasa, M. Kobayashi, Y. Kiyokawa, S. Ota, D. S. Ahn, H. Baba, G. P. A. Berg, M. Dozono, N. Fukuda, T. Furuno, E. Ideguchi, N. Inabe, T. Kawabata, S. Kawase, K. Kisamori, K. Kobayashi, T. Kubo, Y. Kubota, C. S. Lee, M. Matsushita *et al.*, Phys. Rev. Lett. **121**, 022506 (2018).
[14] J. Dobaczewski, W. Nazarewicz, and P.-G. Reinhard, J. Phys. G: Nucl. Part. Phys. **41**, 074001 (2014).
[15] B. H. Wildenthal, Prog. Part. Nucl. Phys. **11**, 5 (1984).
[16] S. R. Stroberg, J. D. Holt, A. Schwenk, and J. Simonis, Phys. Rev. Lett. **126**, 022501 (2021).
[17] K. Hebeler, S. K. Bogner, R. J. Furnstahl, A. Nogga, and A. Schwenk, Phys. Rev. C **83**, 031301(R) (2011).
[18] A. P. Zuker, Phys. Rev. Lett. **90**, 042502 (2003).
[19] A. Gade, J. A. Tostevin, V. Bader, T. Baugher, D. Bazin, J. S. Berryman, B. A. Brown, D. J. Hartley, E. Lunderberg, F. Recchia, S. R. Stroberg, Y. Utsuno, D. Weisshaar, and K. Wimmer, Phys. Rev. C **93**, 031601(R) (2016).
[20] W. Catford, L. Fifield, T. Ophel, N. Orr, D. Weisser, and C. Woods, Nucl. Phys. A **489**, 347 (1988).
[21] L. Coraggio, G. De Gregorio, A. Gargano, N. Itaco, T. Fukui, Y. Z. Ma, and F. R. Xu, Phys. Rev. C **102**, 054326 (2020).
[22] G. Hagen, M. Hjorth-Jensen, G. R. Jansen, R. Machleidt, and T. Papenbrock, Phys. Rev. Lett. **109**, 032502 (2012).
[23] G. Hagen, P. Hagen, H.-W. Hammer, and L. Platter, Phys. Rev. Lett. **111**, 132501 (2013).
[24] H. Hergert, S. K. Bogner, T. D. Morris, S. Binder, A. Calci, J. Langhammer, and R. Roth, Phys. Rev. C **90**, 041302(R) (2014).
[25] G. Hagen, M. Hjorth-Jensen, G. R. Jansen, and T. Papenbrock, Phys. Scr. **91**, 063006 (2016).
[26] J. D. Holt, J. Menéndez, J. Simonis, and A. Schwenk, Phys. Rev. C **90**, 024312 (2014).
[27] O. B. Tarasov, D. S. Ahn, D. Bazin, N. Fukuda, A. Gade, M. Hausmann, N. Inabe, S. Ishikawa, N. Iwasa, K. Kawata, T. Komatsubara, T. Kubo, K. Kusaka, D. J. Morrissey, M. Ohtake, H. Otsu, M. Portillo, T. Sakakibara, H. Sakurai, H. Sato *et al.*, Phys. Rev. Lett. **121**, 022501 (2018).
[28] B. A. Brown, Physics **3**, 104 (2010).
[29] B. A. Brown, Phys. Rev. C **58**, 220 (1998).
[30] Mass Explorer, http://massexplorer.frib.msu.edu/.
[31] J. Bartel, P. Quentin, M. Brack, C. Guet, and H.-B. Hakansson, Nucl. Phys. A **386**, 79 (1982).
[32] M. Kortelainen, T. Lesinski, J. Moré, W. Nazarewicz, J. Sarich, N. Schunck, M. V. Stoitsov, and S. Wild, Phys. Rev. C **82**, 024313 (2010).
[33] A. F. Lisetskiy, B. A. Brown, M. Horoi, and H. Grawe, Phys. Rev. C **70**, 044314 (2004).
[34] L. Neufcourt, Y. Cao, W. Nazarewicz, E. Olsen, and F. Viens, Phys. Rev. Lett. **122**, 062502 (2019).
[35] S. M. Lenzi, F. Nowacki, A. Poves, and K. Sieja, Phys. Rev. C **82**, 054301 (2010).
[36] 31 B. Bharti, P. C. Srivastava, and K. Kaneko, J. Phys. G: Nucl. Part. Phys. **47**, 065105 (2020).